Classification of Cell-types in Myocardial Tissue by Quantification of Physiological Characteristics

Shotaro Kaneko[1], Yuichiro Arima[2], Masahiro Migita[3] and Masashi Toda[3]

[1]Graduate School of Science and Technology, Kumamoto University, Kumamoto, Japan
[2]Developmental Cardiology Laboratory, International Research Center for Medical Sciences,
Kumamoto University, Kumamoto, Japan
[3]Research and Education Institute for Semiconductors and Informatics, Kumamoto University,
Kumamoto, Japan
228d8710@st.kumamoto-u.ac.jp

Abstract

Heart disease is the second leading cause of death in Japan, contributing to 15% of all fatalities. Consequently, there exists a pressing need to unveil the pathogenesis of this disease and develop innovative treatment methods. Traditional analysis methods, however, require a significant amount of man-hours and execution time, while being limited in the amount of information they can obtain due to their reliance on two-dimensional images. In this study, we propose a classification method for three-dimensional quantitative analysis of myocardial tissue that considers the cell-specific features existing in the tissue. Using the proposed method, we extracted the nuclei, cells, and vascular endothelial cell membrane regions, and derived two quantitative indices: coverage and filling rate. The experimental results showed that the coverage rate, which quantifies the features of the nucleus of vascular endothelial cells covered by the vascular endothelial cell membrane, is effective in identifying vascular endothelial cells. In addition, the filling rate, which quantifies the characteristic of cardiomyocytes having a small percentage of nuclei in the total cell volume, has been shown to be effective in the identification of cardiomyocytes.

1 Introduction

Heart disease ranks as the second leading cause of death in Japan, responsible for 15% of all fatalities [1]. The term "heart disease" generally used to refer to the diseases of the heart. Among all the heart-related diseases, heart failure most often results in death (approximately 41%) [2, 3]. While significant progress has been made in drug therapy for heart failure, severe cases often lack

established treatments, with heart transplantation being the only viable option. Unfortunately, Japan faces a shortage of heart transplant donors compared to other countries, resulting in only about 50 transplants occurring annually [4]. Therefore, there is an urgent need to elucidate the pathogenesis of heart failure and develop new treatment methods.

Recent advances in computer technology are expected to shed light on the pathophysiology of heart failure at the cellular level. To achieve this, much research has been focused on cardiomyocytes, the main constituents of the heart. However, due to difficulties in using human cardiomyocytes, studies have been conducted on mouse cardiomyocytes, which are also mammalian. A representative study examined the cross-sectional area of cell nuclei based on microscopy images of mouse cardiomyocytes, captured under conditions resembling heart failure [5]. However, most studies to date have primarily analyzed cardiomyocytes, which are three-dimensional (3D) structures, from a two-dimensional (2D) perspective. Single-cell analysis [6], employing machine learning, was used to unravel the mechanisms underlying cardiomyocyte hypertrophy and failure. However, this approach involves isolating cells from tissues and focusing on each cell individually. Therefore, it is not possible to obtain information on cell shapes within tissues or the positional relationships among cells. While 3D modeling, analyzing, and classification methods exist for cell nuclei and nucleoli [7], these techniques utilize only morphological information, such as volume and surface area, of cell nuclei and nucleoli.

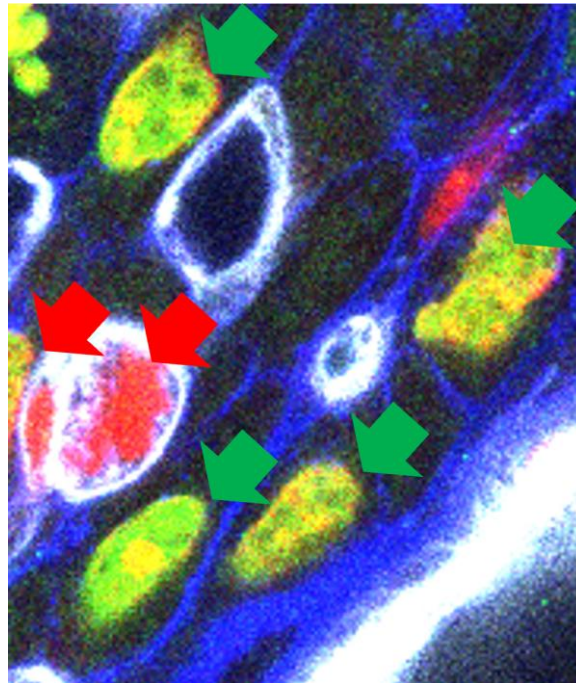In this study, we propose a novel 3D cell classification method designed for mouse myocardial tissue images.

Figure 1: Myocardial tissue microscopy image (red: cell nucleus, green: myocardial cell nucleus, blue: cell membrane, white: vascular endothelial cell membrane, red arrow: vascular endothelial cells, green arrow: myocardial cells, blue arrow: other cells).
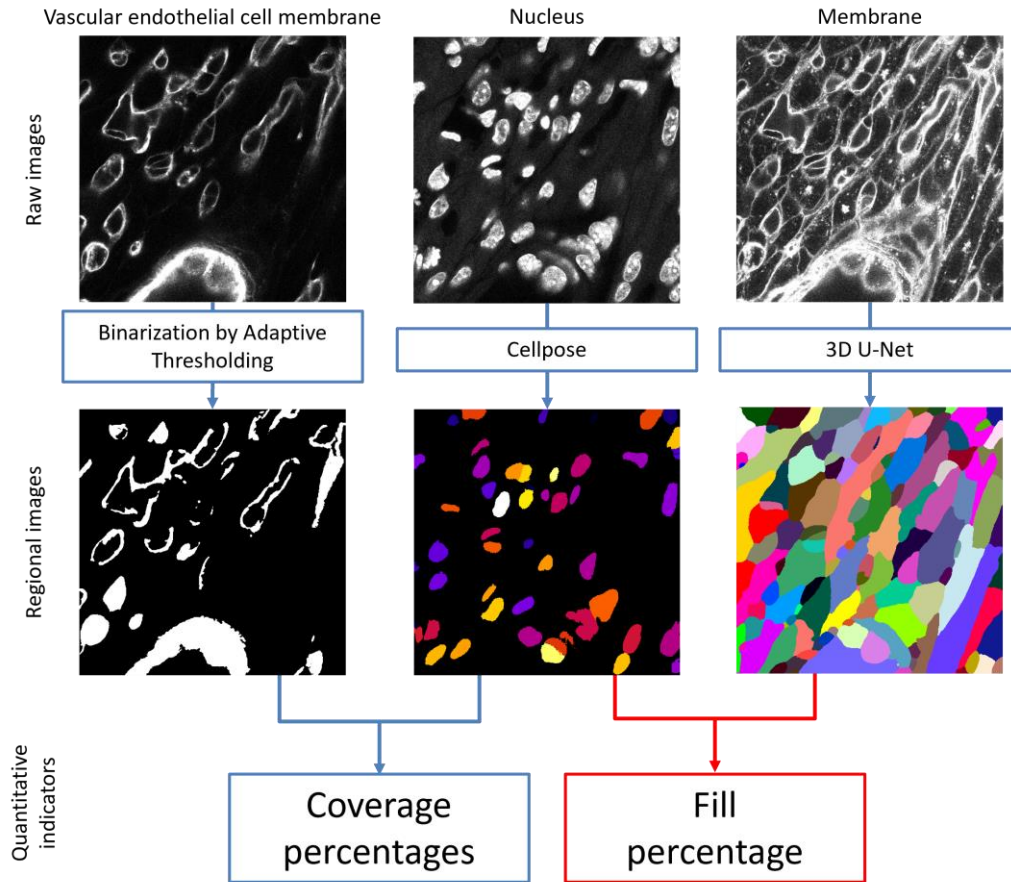
Figure 2: Flow of the proposed method

2 Methods

The heart contains a variety of cells, including myocardial cells, which are the main components of the heart, and vascular endothelial cells, which make up the inner membrane, the innermost membrane of blood vessels. The myocardial tissue microscopic image shown in Figure 1 indicates that vascular endothelial cells are characterized by the cell nucleus and cell membrane being in close contact and the nucleus being covered by the vascular endothelial cell membrane. Cardiomyocytes are characterized by a gap between the cell nucleus and the cell membrane and are not covered by the endothelial cell membrane at all. In this study, we will classify cells based on these characteristics. Figure 2 shows the flow of the cell classification method proposed in this study.

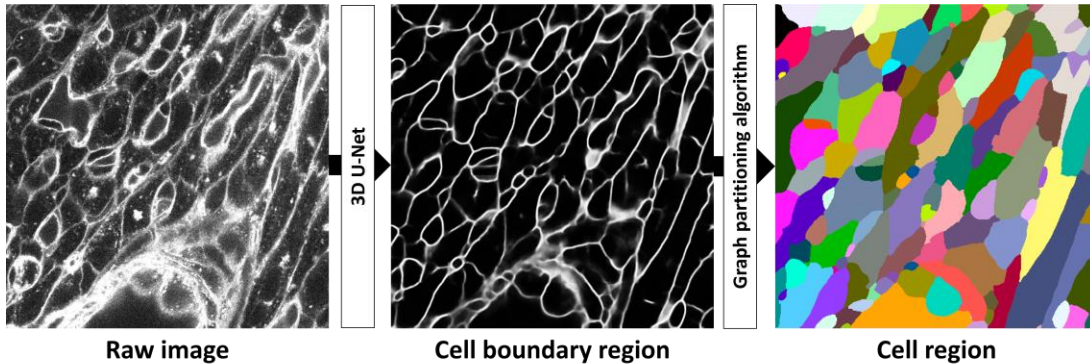## 2.1 Extraction of nuclei, cells, and vascular endothelium

Figure 3: Filling percentages of cardiomyocyte and non-cardiomyocyte.

CellPose [8] is a region extraction method derived from U-Net [9] that can segment a wide range of cell types without the need for parameter adjustments, new training datasets, or model retraining.

Segmentation of the cell membrane is necessary to determine the cellular regions. A 3D U-Net [10, 11], an extension of the 2D operations performed by the conventional U-Net to 3D, was employed to extract the cell membrane regions. PlantSeg [12], a study based on 3D U-Net, focuses on volume segmentation of individual cells from plant tissue images. In this study, we performed instance segmentation of cells based on PlantSeg's method for generating correct images. First, the semi-automatic segmentation of cell boundaries was performed by manually selecting parts of the foreground and background using Autocontext [13] in Ilastik [14]. Next, based on the cell boundaries extracted by Autocontext, Ilastik's Multicut Workflow [15] was used for instance segmentation of the cells and the creation of label images. As the generated label images were incomplete, manual calibration was performed using ITK-SNAP [16]. The cell membrane image and manually-calibrated Ilastik label images were then used to train the 3D U-Net for detecting cell boundaries. Using the graph-partitioning algorithm [17] implemented in PlantSeg on the predicted cell boundaries, cell instance segmentation was obtained. Figure 3 Process was repeated until satisfactory cell region extraction results were obtained, and the final calibration was performed using ITK to extract cytoplasmic regions.
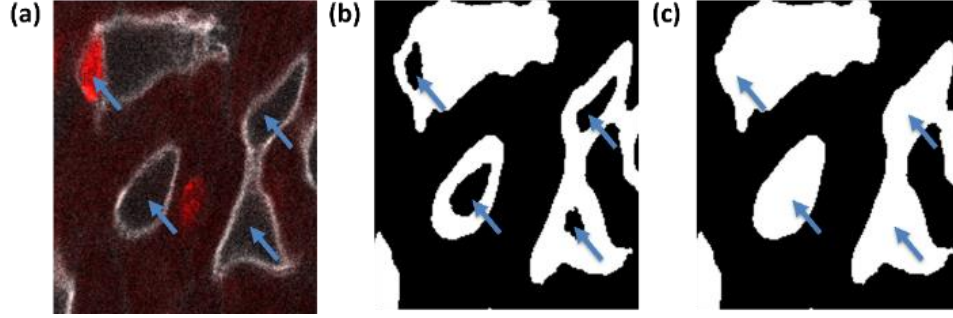
Figure 4: (a) Nucleus (red) and endothelial cell membrane (white), (b) Endothelial area before filling, and (c) Vascular area after hole filling.

The Otsu method, a common binarization method, cannot effectively extract the vascular endothelial region because the endothelial cell membrane has different fluorescence intensity values at different locations. Consequently, adaptive thresholding was employed. After noise reduction and other processes were performed on the binarized image, the endothelial cell nuclei and interior of the blood vessels were not stained and appeared as holes (Figures 4(a) and (b)). Since this makes it difficult to capture the characteristics of the vascular endothelial cells, the closed areas were filled (Figure 4(c)).

2.2   Classification Indicators

In this study, we propose a metric "x", which quantifies the physiological characteristics of each cell type, with the cell classification based on these values.

Vascular endothelial cells are characterized by the fact that the nucleus is covered by the vascular endothelial cell membrane, which is not the case in other cells. To quantify this feature, a coverage P_C was defined and expressed using the following equation:

$$P_C = \frac{n}{m} \times 100, \tag{1}$$

where n is the number of voxels in the vascular endothelium, and m is the number of voxels on the surface of the cell nucleus. The surface voxel of a cell nucleus is defined as a voxel that is not present at any of its x-, y-, or z-coordinate positions. For each voxel constituting a cell nucleus, we search for voxels that make up the endothelial cell membrane region at the same coordinates as the surface voxel of the cell nucleus or within the surrounding 1 voxel (26 connections). Accordinly, if any voxel is found, it is designated as a vascular endothelial voxel.

Compared with non-cardiomyocytes, cardiomyocytes are characterized by a smaller percentage of nuclei in the total cell volume. To quantify this feature, the filling ratio P_F is defined and expressed by the following equation:

$$P_F = \frac{Vn}{Vc} \times 100, \tag{2}$$

where Vn is the volume of the cell nucleus, Vc is the volume of the entire cell, including the nucleus, and the cell corresponding to the nucleus is assumed to exist at the center of gravity of the cell nucleus.

3 Results

3.1 Cell nucleus classification

Two types of images were used in the experiment: images stained with cardiac myocyte nuclei (Sample 1) and images stained with vascular endothelial cell membranes (Sample 2). Therefore, Sample 1 was classified into cardiomyocyte and non-cardiomyocyte nuclei, and Sample 2 was classified into vascular endothelial cell and non-vascular endothelial cell nuclei, and their accuracy was evaluated. Only coverage was used here, and the classification was based on the threshold values derived by discriminant analysis. Table 1 presents the classification accuracy evaluation results for Samples 1 and 2. The results for Sample 1 showcased that although myocardial cell nuclei were rarely missed, false positives (FPs) occurred in above half of the cases. The results for Sample 2 indicated that FPs for vascular endothelial cell nuclei were suppressed, but above 30% of them were missed.

Sample name	Accuracy	Precision	Recall	F-measure
Sample 1	0.644	0.463	0.987	0.631
Sample 2	0.811	0.802	0.685	0.739

Table 1: Assessing the accuracy of cell nucleus classification.

3.2 Comparison of filling rates of cardiomyocytes and non-cardiomyocytes

Figure 5 illustrates the distribution of the filling rates of cardiomyocytes and noncardiomyocytes in Sample 1. It can be observed that the filling ratio of cardiomyocytes is predominantly below 40%, while the filling ratio of noncardiomyocytes varies widely. This discrepancy arises because the nucleus occupies a smaller percentage of the total cell volume in cardiomyocytes compared to non-cardiomyocytes, making the filling ratio a potentially useful feature for identifying cardiomyocytes with high accuracy.
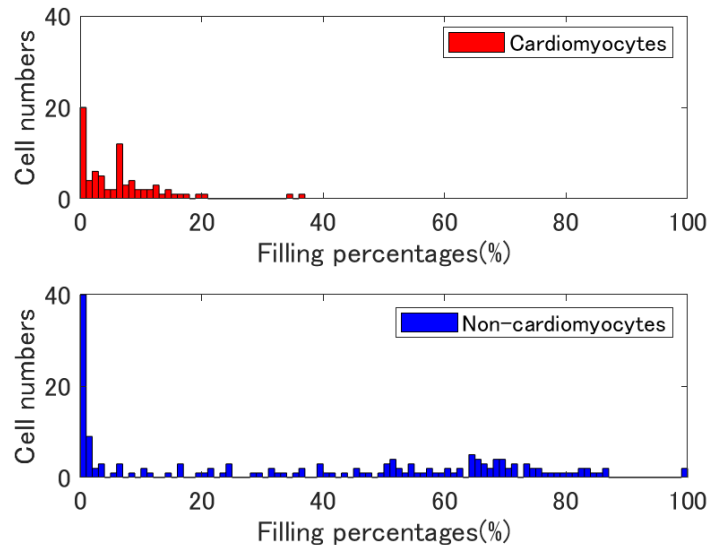

Figure 5: Cardiomyocyte and non-cardiomyocyte filling percentages.

4 Conclusions

In this study, we proposed a method for the segmentation and cell classification of mouse myocardial tissue in 3D. The 3D U-Net-based segmentation of the myocardial tissue demonstrated that it is possible to accurately extract cell membrane regions with varying brightness values from different locations. Cell classification was based on the coverage ratio, which quantifies the characteristics of the nucleus covered by the vascular endothelial cell membrane. The reproducibility of Sample 1 (0.987) and the fitness rate of Sample 2 (0.802) suggest that the coverage ratio is effective for cell classification, as it captures the feature that the nucleus of cardiomyocytes is not covered by the vascular endothelial cell membrane, while that of vascular endothelial cells is covered by the endothelial cell membrane. However, the fitness rate of sample 1 was 0.463, indicating that more than half of the cardiomyocyte nuclei were FPs. Therefore, it is necessary to introduce a more useful index to improve the classification accuracy. The filling ratio, which is related to the cell volume of the cardiomyocyte, may prove useful in accurately identifying cardiomyocytes.

For the future segmentation of myocardial tissue using 3D U-Net, we aim to improve the accuracy of cell boundary prediction and cell instance segmentation by increasing the training data. In addition, since only nuclei can be classified at this stage, introducing cell instance segmentation results using 3D U-Net will enable cell classification.

References

[1] "Ministry of Health, Labour and Welfare, Summary of the 2020 Vital Statistics Monthly Report Annual Total (Approximate)," [Online]. Available: https://www.mhlw.go.jp/toukei/saikin/hw/jinkou/geppo/nengai20/dl/gaikyouR2.pdf.

[2] "What is Cardiac Disease? Four typical types and their treatment - Asahi Mutual Life Insurance Co.," [Online]. Available: https://www.asahi-life.co.jp/nethoken/howto/seikatsu/heart-disease-typical-types.html.

[3] "Epidemiology of heart failure and ischemic heart disease," [Online]. Available: https://www.ncvc.go.jp/coronary2/column/20211209_05.html.

[4] K. Kinugawa, "Current status and future prospects of heart failure treatment by stage," [Online]. Available: https://www.jstage.jst.go.jp/article/naika/108/3/108_527/_pdf.

[5] W Bao N. Puente, Wataru Kimura, Shalini A. Muralidhar, et al, "The Oxygen Rich Postnatal Environment Induces Cardiomyocyte Cell Cycle Arrest Through DNA Damage Response," Cell, 2014.

[6] Nomura, S., Satoh, M., Fujita, T. et al, "Cardiomyocyte gene programs encoding morphological and functional signatures in cardiac hypertrophy and failure," Nature Communications, 2018.

[7] Alexandr A. Kalinin., Ari Allyn-Feuer., Alex Ade., et al, "3D Shape Modeling for Cell Nuclear Morphological Analysis and Classification," Scientific Reports, 2018.

[8] Stringer, C., Wang, T., Michaelos, M. et al, "Cellpose: a generalist algorithm for cellular segmentation," bioRxiv, 2020.

[9] Ronneberger, O., Fischer, P., Brox, T, "U-Net: Convolutional Networks for Biomedical Image Segmentation," arXiv, 2015.

[10] Çiçek, Ö., Abdulkadir, A., Lienkamp, S.S., Brox, T., Ronneberger, O, "3D U-Net: Learning Dense Volumetric Segmentation from Sparse Annotation," arXiv, 2016.

[11] "wolny/pytorch-3dunet: 3D   U-Net   model,"   [Online].   Available: https://github.com/wolny/pytorch-3dunet.

[12] Wolny, A., Cerrone, L., Vijayan, A. et al, "Accurate and versatile 3D segmentation of plant tissues at cellular resolution," eLife, 2020.

[13] Berg, S., Kutra, D., Kroeger, T. et al, "ilastik: interactive machine learning for (bio)image analysis," *Nat Methods,* no. 16, p. 1226–1232, 2019.

[14] Tu, Z Bai X, "Auto-context and its application to high-level vision tasks and 3d brain image segmentation," *IEEE,* p. 1744–1757, 2010.

[15] Beier, T., Pape, C., Rahaman, N. et al, "Multicut brings automated neurite segmentation closer to human performance," *Nat Methods,* no. 14, pp. 101-102, 2017.

[16] H. a. Paul A. Yushkevich and Joseph Piven and Cody Hazlett, "User-Guided 3D Active Contour Segmentation of Anatomical Structures: Significantly Improved Efficiency and Reliability," *Neuroimage,* vol. 31, no. 3, pp. 1116–1128, 2006.

[17] Kappes, J.H., Speth, M., Andres, B., Reinelt, G., Schn, C, "Globally Optimal Image Partitioning by Multicuts," *EMMCVPR,* vol. 6819, 2011.